Original Article

Quantitative parameters of static imaging and fast kinetics imaging in ^{18}F-FDG total-body PET/CT for the assessment of histological feature of pulmonary lesions

Nan Meng[1,2#], Meng Zhang[3#], Jipeng Ren[3], Fangfang Fu[1], Beichen Xie[3], Yaping Wu[1], Zhong Li[3], Bo Dai[1], Yuxia Li[3], Tao Feng[4], Tianyi Xu[5], Meiyun Wang[1,2]

[1]Department of Medical Imaging, Henan Provincial People's Hospital & Zhengzhou University People's Hospital, Zhengzhou, China; [2]Laboratory of Brain Science and Brain-Like Intelligence Technology, Biomedical Research Institute, Henan Academy of Sciences, Zhengzhou, China; [3]Department of MR, The First Affiliated Hospital, Xinxiang Medical University, Weihui, China; [4]United Imaging Healthcare America Inc. TX, USA; [5]United Imaging Healthcare, Shanghai, China

Contributions: (I) Conception and design: M Wang; (II) Administrative support: M Wang, F Fu, Y Wu; (III) Provision of study materials or patients: M Zhang, N Meng, J Ren, Z Li; (IV) Collection and assembly of data: N Meng, F Fu, B Dai, Y Wu; (V) Data analysis and interpretation: Y Li, B Xie, T Xu, T Feng; (VI) Manuscript writing: All authors; (VII) Final approval of manuscript: All authors.

[#]These authors contributed equally to this work and should be considered as co-first authors.

Correspondence to: Meiyun Wang, MD, PhD. Department of Medical Imaging, Henan Provincial People's Hospital & Zhengzhou University People's Hospital, 7 Weiwu Road, Zhengzhou 450000, China. Email: mywang@zzu.edu.cn.

Background: To investigate the value of quantitative parameters related to static imaging and fast kinetics imaging of total-body (TB) 2-[^{18}F]-fluoro-2-deoxy-D-glucose (^{18}F-FDG) positron emission tomography/computed tomography (PET/CT) in differentiating benign from malignant pulmonary lesions and squamous cell carcinoma (SCC) from adenocarcinoma (AC) and to analyze the correlation of each parameter with the Ki-67 index.

Methods: A total of 108 patients with pulmonary lesions from July 2021 to May 2022 in the Henan Provincial People's Hospital, China, were consecutively recruited for TB ^{18}F-FDG PET/CT in this prospective study. Static imaging parameters maximum standardized uptake value (SUV_{max}) and fast kinetics imaging parameters transport constant (K_1), rate constants (k_2), time delay (t_d), and fractional blood volume (v_b) were calculated and compared. The area under the receiver operating characteristic (ROC) curve (AUC), Delong test, Logistic regression analyses, and Pearson correlation were used to assess diagnostic efficacy, find independent predictors and analyse correlations respectively.

Results: Malignant lesions had higher SUV_{max} and K_1 and lower v_b than benign lesions, and SCC had higher SUV_{max} and K_1 and lower t_d and v_b than AC (all P<0.05). For the differentiation of benign and malignant lesions, SUV_{max}, K_1, and v_b were independent predictors, and AUC (SUV_{max} + K_1+ v_b) =0.909 (95% CI: 0.839–0.956), AUC (SUV_{max}) =0.883 (95% CI: 0.807–0.937), AUC (K_1) =0.810 (95% CI: 0.723–0.879), and AUC (v_b) =0.746 (95% CI: 0.653–0.825), where AUC (SUV_{max} + K_1+ v_b) was significantly different from AUC (K_1), AUC (v_b) (Z=3.006, 3.965, all P<0.05). For the differentiation of SCC and AC, SUV_{max}, K_1, t_d, and v_b were independent predictors, and AUC (SUV_{max} + K_1+ t_d + v_b) =0.946 (95% CI: 0.840–0.991), AUC (SUV_{max}) =0.818 (95% CI: 0.680–0.914), AUC (K_1) =0.770 (95% CI: 0.626–0.879), AUC (v_b) =0.737 (95% CI: 0.590–0.853), and AUC (t_d) =0.669 (95% CI: 0.510–0.791), where AUC (SUV_{max} + K_1+ t_d + v_b) was significantly different from AUC (SUV_{max}), AUC (K_1), AUC (v_b), and AUC (t_d) (Z=2.269, 2.821, 2.848, and 3.276, all P<0.05). SUV_{max} and K_1 were moderately and mildly positively correlated with the Ki-67 index (r=0.541, 0.452, all P<0.05), respectively.

Conclusions: Quantitative parameters of static imaging and fast kinetics imaging in ^{18}F-FDG total-body

PET/CT can be used to differentiate benign from malignant pulmonary lesions and SCC from AC and to assess Ki-67 expression.

Keywords: Pulmonary lesions; total-body positron emission tomography/computed tomography (TB PET/CT); fast kinetics parametric imaging

Submitted Feb 15, 2023. Accepted for publication Jun 30, 2023. Published online Aug 07, 2023.
doi: 10.21037/qims-23-186
View this article at: https://dx.doi.org/10.21037/qims-23-186

Introduction

Pulmonary cancer is the most common malignancy worldwide, and is considered the leading cause of cancer-related deaths globally (1). As an accurate noninvasive imaging method, positron emission tomography/computed tomography (PET/CT) with 2-[^{18}F]-fluoro-2-deoxy-D-glucose (^{18}F-FDG) has received widespread clinical recognition for the diagnosis and evaluation of pulmonary lesions (2-4). In clinical practice, a PET/CT examination is currently mainly performed as static imaging, and the data are evaluated in units of standardized uptake value (SUV) (5,6). However, due to factors such as plasma glucose level, body composition, lesion type, and scan time, the semiquantitative indicator SUV not only always has great variability but also low specificity for malignant lesions (7,8).

Dynamic PET imaging can reflect the kinetic spatial distribution process of the tracer to provide more detailed quantitative information on the metabolic properties of the target tissue than conventional static PET (9,10). Several studies have demonstrated the reliability of this approach in improving the contrast and detectability of the lesion (11,12). However, dynamic PET imaging has not been widely applied in the clinic, partly because of the long duration of dynamic protocols that often leads to patient discomfort and motion and partly due to the limited axial extent (15–25 cm) of conventional scanners, which often results in inadequate coverage or a decreased signal-to-noise ratio (13,14). The advent of the total-body (TB) PET/CT scanner has ushered a new era of PET imaging (15). The 194-cm-long axial field of view not only covers the patient's entire body but also brings up to 40× and 6× improvements in effective sensitivity and the signal-to-noise ratio, respectively (16,17). With these advantages, it becomes feasible to obtain high-quality information on the static and dynamic distribution of tracers in a short period using a TB PET/CT scanner (18). Nevertheless, currently, the commonly used dynamic scanning protocols, such as Patlak analysis (19) and Logan analysis (20), usually require a scan time of at least 30 minutes, making them difficult to incorporate into routine clinical applications. Recently, Feng *et al.* proposed a new kinetics parametric imaging method based on TB PET/CT, which not only works at a fast imaging speed, but can also reconstruct some kinetic parameters to achieve similar evaluation results as the traditional methods (21). Currently, a small number of studies have evaluated pulmonary lesions using dynamic imaging with TB PET/CT, but the subjects in these studies were with metastatic lymph nodes and the dynamic models they used were all conventional Patlak model with long scan duration (12,22).

The purpose of this study was to investigate the value of quantitative parameters related to static imaging and fast kinetics imaging of TB ^{18}F-FDG PET/CT in differentiating benign from malignant pulmonary lesions, squamous cell carcinoma (SCC) from adenocarcinoma (AC), and to analyze the correlation of each parameter with the Ki-67 index, in turn providing new insights for the clinical diagnosis and prognostic assessment of lung cancer patients. We present this article in accordance with the STARD reporting checklist (available at https://qims.amegroups.com/article/view/10.21037/qims-23-186/rc).

Methods

Study population

The study was conducted in accordance with the Declaration of Helsinki (as revised in 2013). This prospective study complied with ethical committee standards and was approved by the ethics committee of the Henan Provincial People's Hospital & Zhengzhou University People's Hospital (No. 2018067) and all participants gave informed written consent. From July 2021 to May 2022, a consecutive series of 126 patients with pulmonary lesions were enrolled for TB ^{18}F-FDG PET/

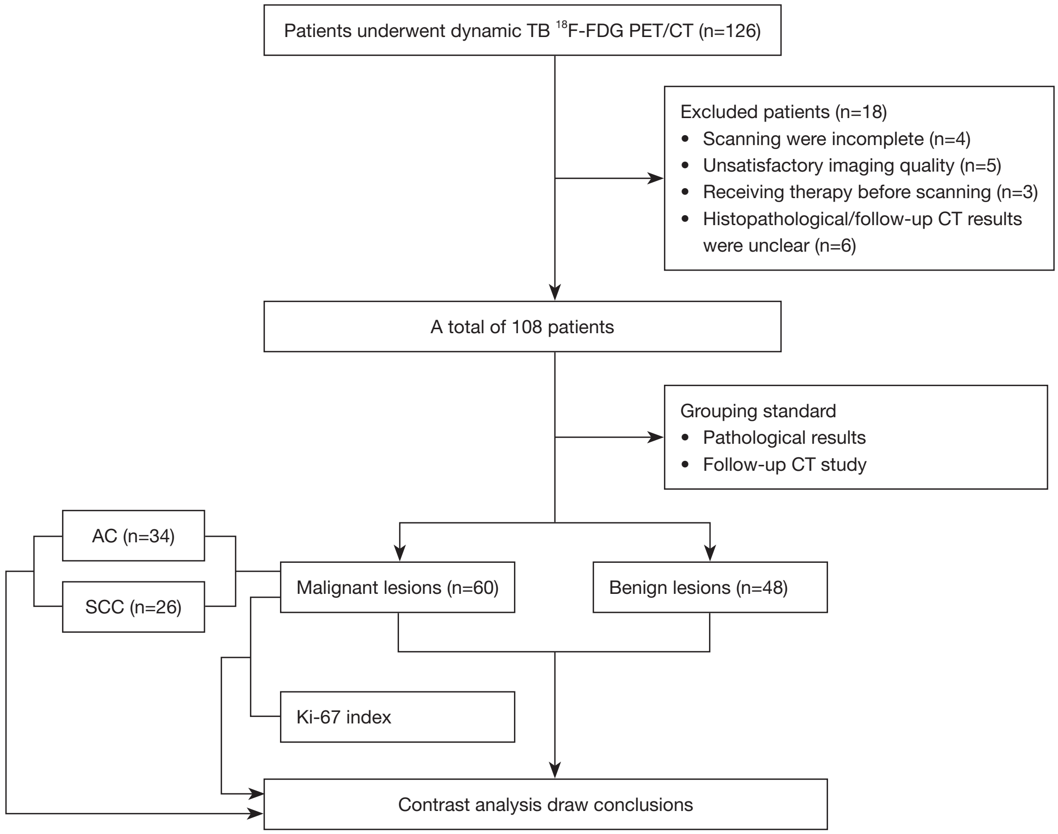

Figure 1 Flow diagram of the patient selection process. SCC, squamous cell carcinoma; AC, adenocarcinoma.

CT in this study. The exclusion criteria were as follows: (I) patients who had not undergone scanning with all imaging sequences due to physical symptoms (n=4); (II) patients whose image quality was poor making it difficult to perform dynamic analysis (n=5); (III) patients who underwent chemotherapy, radiotherapy, or surgery before scanning (n=3); and (IV) patients without definitive pathological or follow-up CT results (n=6). Ultimately, a total of 108 patients with pulmonary lesions were included for this research (*Figure 1*).

Image acquisition

A TB ^{18}F-FDG PET/CT scanner (uEXPLORER, UIH, Shanghai, China) was used in this study, the specific configuration parameters of which can be found in previous research (15,18). ^{18}F-FDG was produced by a FracerLab FX-FDG (GE Minitrac) with a purity >95% and a pH of 4.5–8.5. All patients fasted for at least 6 hours prior to the scan to ensure that their serum glucose levels were <6.5 mmol/L at the time of ^{18}F-FDG injection. During the scan, all patients were placed in a feet-first supine position, and the patient's legs and elbows were secured with straps to minimize patient movement. An attenuation correction CT was performed first with an 80 kV tube voltage and 20 mA tube current for PET image localization and reconstruction. Then, the kinetics parametric imaging protocol was started at the same time as a bolus of ^{18}F-FDG (4.07 MBq/kg) was injected by hand into a vein in the patient's leg, preferably into the leg with less varicosity. The diagnostic CT was performed last (120 kV, 160 mAs). The reconstructions of dynamic images were performed using a 192×192 matrix, with both time-of-flight (TOF) and point spread function (PSF), using 20 subsets and 3 iterations. The scatter, attenuation, randoms, and normalization corrections were also included in the reconstruction process. Noise suppression of reconstructed images was handled by a 3D Gaussian filter with full width at half maximum of 6 mm.

Parameters generation

Collected dynamic data were analyzed by using a housedeveloped software package (https://jnm.snmjournals.org/content/62/5/738.abstract). Kinetics parametric images based on a nonlinear one-compartment model were generated with the following formula:

$$C(t) = v_b C_b(t - t_d) + K_1 \exp(-k_2 t) \otimes C_p(t - t_d) \quad [1]$$

where K_1 and k_2 are the forward and backward transport rates of ^{18}F-FDG from plasma to tissue, respectively, v_b is the blood fraction in the tissue, t_d is the voxel-dependent delay time, C(t) indicates the concentration of ^{18}F-FDG in the tissue, $C_b(t)$ is the time-activity-curve (TAC) for the whole blood, $C_p(t)$ is the plasma input function and $\otimes$ represents the convolution operation. The specific derivation of this equation has been described in detail in a previous study (21). To obtain image-derived input functions, the volumes of interest (VOI) of the left ventricle and ascending aorta was plotted on PET/CT images and TAC was obtained (23). The VOI of the ascending aorta has a diameter of 16 mm and a height of 40 mm. The left ventricle boundaries were excluded from the left ventricle VOI to minimize the influence of respiratory motion, and the total volume was approximately similar to that of the ascending aortic VOI. Whole blood-plasma correction was applied on TAC $C_b(t)$ to estimate the plasma input function $C_p(t)$. K_1, k_2, t_d, and v_b were estimated by an alternate update approach with 18 main iterations. Within each iteration, K_1 and v_b were first updated with fixed k_2 and t_d with 9 subiterations, k_2 was updated with fixed K_1, v_b, and t_d with 1 subiteration, followed by the update of t_d with fixed K_1, k_2, and v_b using 3 subiterations (24).

For static PET, the scan was started 60 minutes after ^{18}F-FDG injection, the scan time was 5 minutes (25), and the following formula was applied:

$$SUV(t) = \frac{C(t)}{\text{injected dose/body weight}} \quad [2]$$

After processing, all parametric images were transferred to a workstation (uWS-MI, R001, UIH, Shanghai, China). The fused PET/CT software of the workstation was able to semi-automatically extract the VOI of pulmonary lesions from the static PET image and generate SUV_{max} value, and then mapped the VOI to different parameter maps of the fast kinetics imaging to generate K_1, k_2, $t_{d,}$ and v_b values. Two nuclear medicine physicians (NM and FF, with 6 and 15 years of experience, respectively) independently generated the values of the above parameters for each lesion and were unaware of each other's results as well as the clinical data and pathology reports.

Reference standards

The specimens of 60 malignant lesions and 25 benign lesions were obtained by biopsy or surgery within 2 weeks of the examination, and the remaining 23 benign lesions were finally diagnosed based on follow-up CT (follow-up period; 5–20 weeks) without biopsy or surgery. Hematoxylin/eosin (HE) staining was used to determine the histological type. A murine Ki-67 monoclonal antibody (MIB-1, DAKO, Denmark) was used to determine the Ki-67 index. Five hotspots (areas with a high number of positive cells) were selected at 400× magnification for counting 100 tumor cells each, and the proportion of positive cells within them was counted as an indication of Ki-67 expression.

Statistical analysis

MedCalc (Version 15.0; MedCalc Software) and SPSS (Version 23.0; IBM) software were used for statistical analysis. Interobserver reliability between the 2 readers was described with the intraclass correlation coefficient (ICC) ($r \geq 0.75$, excellent; $0.60 \leq r < 0.75$, good; $0.40 \leq r < 0.60$, fair; and $r < 0.40$, poor) (26). Continuous variables were subsequently described as their mean ± standard deviation. The Shapiro-Wilk test was utilized to determine if the data conformed to a normal distribution. The independent sample *t*-test and Mann-Whitney U test were used for normally and non-normally distributed data, respectively. Categorical variables were described as their totals and percentages. Receiver operating characteristic (ROC) curves were generated to describe diagnostic efficacy, and the Delong test was applied to identify differences in the area under the ROC curve (AUC) of different parameters. Logistic regression analyses were performed to identify independent factors and to explore the combination diagnosis. Pearson correlations were employed to describe the correlation ($r \geq 0.75$, good; $0.50 \leq r < 0.75$, moderate; $0.25 \leq r < 0.50$, mild; and $r < 0.25$, little or none) (27). A $P < 0.05$ (two-tailed test) was considered statistically significant.

Results

Patients characteristics

A total of 108 patients with pulmonary lesions were included in this study, with an average age of 57.29±10.13 years,

Table 1 Clinicopathologic characteristics of patients

Variable	Benign	Malignant
Age (years)	58.77±10.11	56.10±10.07
Maximum diameter (mm)	40.16±23.78	34.67±14.68
Number of lesions	48	60
Smoking	24 (50.00)	28 (46.67)
Male	25 (52.08)	31 (51.67)
Types of lesions		
Bronchopneumonia	10 (20.83)	–
Organizing pneumonia	8 (16.67)	–
Pulmonary tuberculosis	7 (14.58)	–
Post-inflammatory scar	5 (10.42)	–
Inflammatory pseudotumor	6 (12.50)	–
Inflammatory granuloma	4 (8.33)	–
Hamartoma	3 (6.25)	–
Fungal infection	5 (10.42)	–
Squamous cell carcinoma	–	26 (43.33)
Adenocarcinoma	–	34 (56.67)
TNM stage		
I	–	6 (10.00)
II	–	30 (50.00)
III	–	19 (31.67)
IV	–	5 (8.33)
Ki-67 index		
≤10% (–)	–	10 (16.67)
11–25% (+)	–	12 (20.00)
26–50% (++)	–	22 (36.67)
≥51% (+++)	–	16 (26.66)

Continuous variables were subsequently described as their mean ± standard deviation. Categorical variables were described as their totals and percentages. TNM, tumor node metastasis.

including 56 males, 52 females, 48 benign lesions and 60 malignant lesions, and 52 smokers and 56 non-smokers. The clinicopathological and imaging characteristics are shown in *Table 1* and *Figure 2*, respectively.

Consistency test

The data measured by the 2 readers had excellent consistency (all ICCs >0.75). Therefore, the 2 readers' mean results of each parameter were used for statistical analyses.

Comparison of parameters

Malignant lesions had higher SUV_{max} (5.73±3.69 *vs.* 1.84±1.29) and K_1 (3.51±1.82 *vs.* 1.86±0.92) and lower v_b (7.82±5.85 *vs.* 13.85±6.93) than benign lesions (all P<0.001), and SCC had higher SUV_{max} (7.51±2.73 *vs.* 4.33±2.18) and K_1 (4.19±1.21 *vs.* 2.93±1.58) and lower t_d (–28.09±25.07 *vs.*

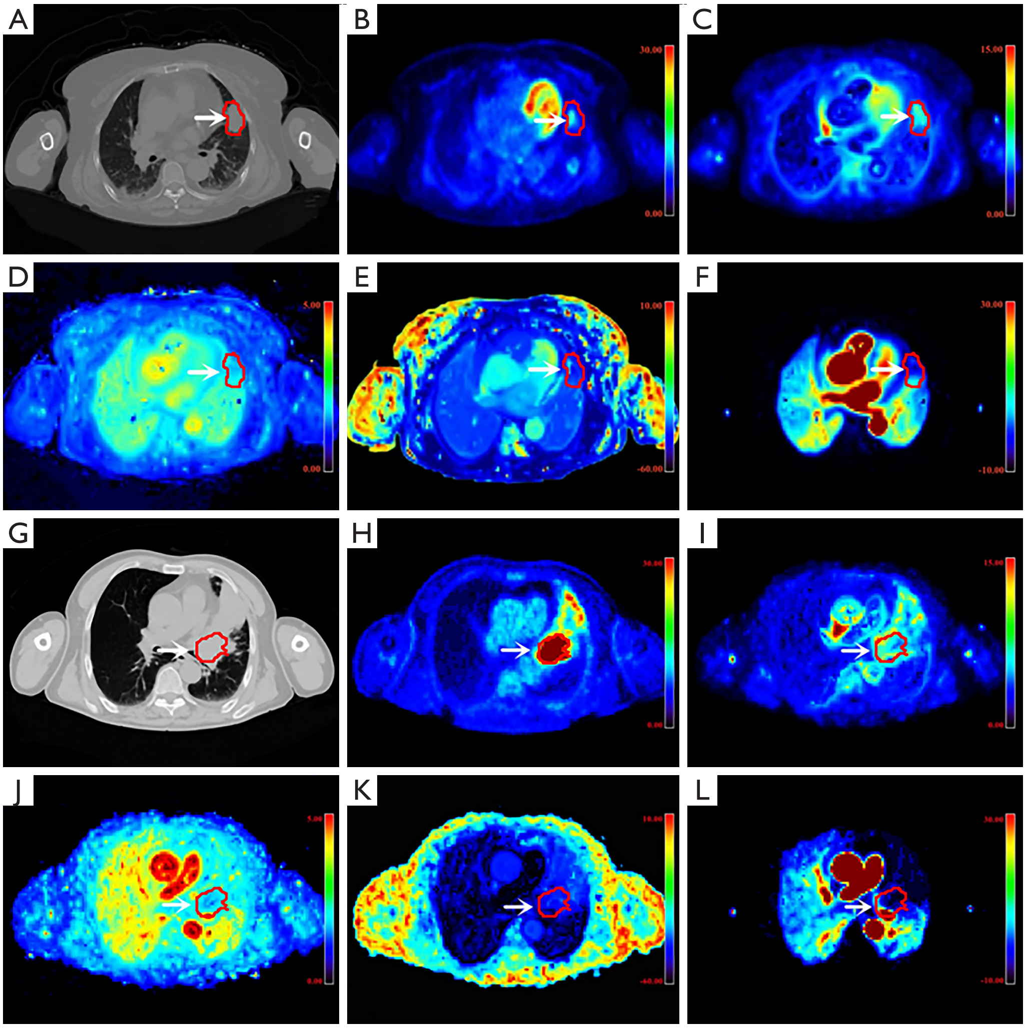

Figure 2 The ^{18}F-FDG total-body PET/CT scans in pulmonary lesion patient. (A-F) A 55-year-old woman with left pulmonary pneumonia (white arrowheads); (G-L) a 71-year-old man with left pulmonary squamous cell carcinoma (white arrowheads). (A,G) Axial images of CT; (B,H) axial reconstructed images of SUV; (C,I) axial reconstructed images of K_1; (D,J) axial reconstructed images of k_2; (E,K) Axial reconstructed images of t_d; and (F,L) axial reconstructed images of v_b. ^{18}F-FDG PET/CT, 2-[^{18}F]-fluoro-2-deoxy-D-glucose positron emission tomography/computed tomography; SUV, standardized uptake value; K_1, the forward transport rates of ^{18}F-FDG from plasma to tissue; k_2, the backward transport rates of ^{18}F-FDG from plasma to tissue; v_b, the blood fraction in the tissue; t_d, the voxel-dependent delay time.

−10.91±26.57) and v_b (4.76±5.16 *vs.* 9.19±5.42) than AC (P<0.001, P=0.002, P=0.031, and P=0.006, respectively). There were no significant differences in k_2 and t_d between malignant and benign lesions or in k_2 between SCC and AC (P=0.098, 0.400, and 0.085, respectively) (*Table 2*, *Figure 3*).

Regression analyses

Age, sex, smoking status, maximum diameter, and related parameters were all included in the analyses. In the identification of malignant and benign lesions, univariate analysis showed that SUV_{max}, K_1, k_2, and v_b were predictors (OR =0.437, 0.356, 2.325, and 1.158, P<0.001, P<0.001, P=0.096, and P<0.001, respectively), and multivariate analysis revealed that only SUV_{max}, K_1, and v_b were independent predictors (OR =0.519, 0.558, and 1.118, P<0.001, P=0.029, and P=0.035, respectively). In the identification of SCC and AC, univariate analysis showed that SUV_{max}, K_1, t_d, and v_b were predictors (OR =1.664, 1.805, 0.971, and 0.838, P=0.001, 0.012, 0.040, and 0.016,

Table 2 Comparison of different parameters among different groups

Parameters	Malignant *vs*. Benign				SCC *vs*. AC			
	Malignant	Benign	t/z value	P value	SCC	AC	t/z value	P value
SUV_{max}	5.73±3.69	1.84±1.29	−6.814	<0.001[a]	7.51±2.73	4.33±2.18	−4.207	<0.001[a]
K_1 (×10^{-3} mL/g/s)	3.51±1.82	1.86±0.92	−5.521	<0.001[a]	4.19±1.21	2.93±1.58	−3.109	0.002[a]
k_2 (×10^{-2} s^{-1})	1.69±0.38	1.82±0.42	−1.674	0.098[b]	1.57±0.46	1.72±0.33	−1.725	0.085[b]
t_d (s)	−17.78±27.68	−11.23±29.19	−0.841	0.400[a]	−28.09±25.07	−10.91±26.57	2.248	0.031[a]
v_b (×10^{-2})	7.82±5.85	13.85±6.93	−4.812	<0.001[b]	4.76±5.16	9.19±5.42	−2.726	0.006[b]

Continuous variables were subsequently described as their mean ± standard deviation. Categorical variables were described as their totals and percentages. [a], Comparisons were performed by Mann-Whitney U test; [b], Comparisons were performed by independent *t* test. AC, adenocarcinoma; SCC, squamous cell carcinoma; SUV_{max}, maximum standardized uptake value; K_1, the forward transport rates of ^{18}F-FDG from plasma to tissue; k_2, the backward transport rates of ^{18}F-FDG from plasma to tissue; v_b, the blood fraction in the tissue; t_d, the voxel-dependent delay time.

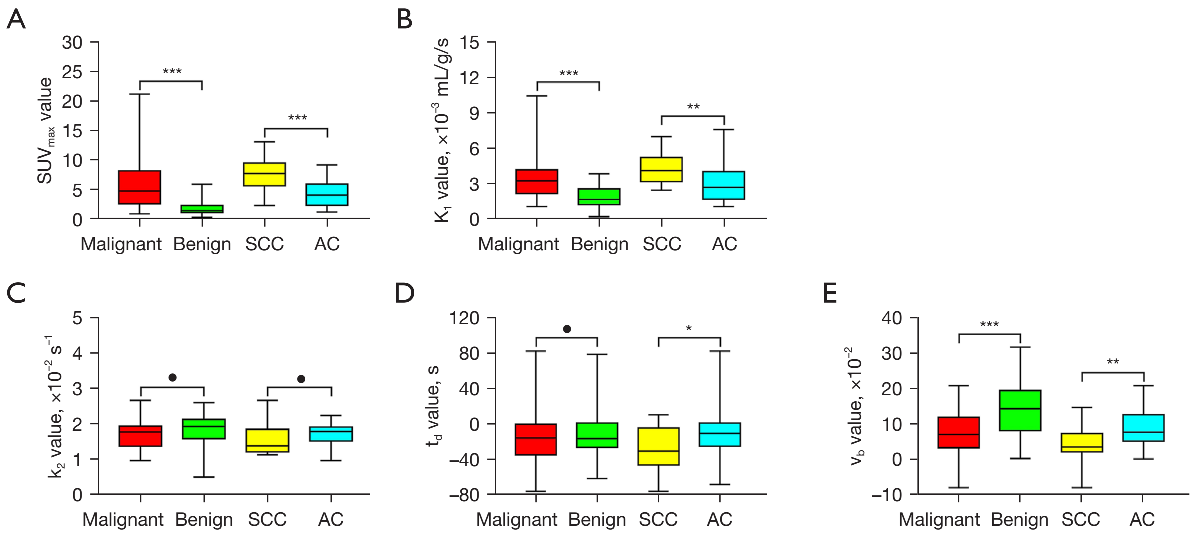

Figure 3 Box plot of different parameters. (A-E) represent SUV_{max}, K_1, k_2, t_d, and v_b, respectively. *, P<0.05; **, P<0.01; ***, P<0.001; •, P>0.05. SUV_{max}, maximum standardized uptake value; K_1, the forward transport rates of ^{18}F-FDG from plasma to tissue; k_2, the backward transport rates of ^{18}F-FDG from plasma to tissue; v_b, the blood fraction in the tissue; t_d, the voxel-dependent delay time.

respectively), and multivariate analysis revealed that SUV_{max}, K_1, t_d, and v_b were independent predictors (OR =1.874, 3.884, 0.935, and 0.664, P=0.013, 0.030, 0.020, and 0.027, respectively) (*Table 3*).

Diagnostic performance of different parameters

For the differentiation of malignant and benign lesions, the AUCs of the combination of independent predictors (SUV_{max} + K_1+ v_b), SUV_{max}, K_1, and v_b were 0.909, 0.883, 0.810, and 0.746, respectively, and the differences between AUC (SUV_{max} + K_1+ v_b) and AUC (K_1), and AUC (v_b) were significant (Z=3.006, 3.965, all P<0.05). When individual parameters were assessed, there was no significant difference in AUC among different parameters (all P>0.05). For the differentiation of SCC and AC, the AUCs of the combination of independent predictors (SUV_{max} + K_1+ v_b + t_d), SUV_{max}, K_1, v_b, and t_d were 0.946, 0.818, 0.770, 0.737, and 0.669, respectively, and the differences between AUC (SUV_{max} + K_1+ t_d + v_b) and AUC (SUV_{max}), AUC (K_1), AUC

Table 3 Univariate and multivariate analyses

Parameters	Univariate analyses		Multivariate analyses	
	OR (95% CI)	P	OR (95% CI)	P
Malignant *vs.* benign				
Age	1.028 (0.988–1.069)	0.176	–	–
Sex	0.379 (0.097–1.474)	0.162	–	–
Smoking	1.152 (0.348–3.812)	0.817	–	–
Maximum diameter (mm)	1.162 (0.948–1.425)	0.149	–	–
SUV_{max}	0.437 (0.311–0.613)	<0.001	0.519 (0.368–0.733)	<0.001
K_1 ($\times10^{-3}$ mL/g/s)	0.356 (0.230–0.553)	<0.001	0.558 (0.331–0.941)	0.029
k_2 ($\times10^{-2}$ s^{-1})	2.325 (0.861–6.274)	0.096	0.707 (0.136–3.671)	0.680
t_d (s)	1.008 (0.995–1.022)	0.237	–	–
v_b ($\times10^{-2}$)	1.158 (1.080–1.242)	<0.001	1.118 (1.008–1.241)	0.035
SCC *vs.* AC				
Age	1.015 (0.955–1.078)	0.630	–	–
Sex	1.143 (0.355–3.681)	0.823	–	–
Smoking	1.571 (0.479–5.153)	0.456	–	–
Maximum diameter (mm)	1.388 (0.923–2.087)	0.115	–	–
SUV_{max}	1.664 (1.230–2.250)	0.001	1.874 (1.144–3.069)	0.013
K_1 ($\times10^{-3}$ mL/g/s)	1.805 (1.137–2.863)	0.012	3.884 (1.137–13.269)	0.030
k_2 ($\times10^{-2}$ s^{-1})	0.343 (0.067–1.755)	0.199	–	–
t_d (s)	0.971 (0.944–0.999)	0.040	0.935 (0.883–0.990)	0.020
v_b ($\times10^{-2}$)	0.838 (0.726–0.968)	0.016	0.664 (0.461–0.955)	0.027

All factors with P<0.1 in univariate analyses were included in multivariate regression analyses. AC, adenocarcinoma; SCC, squamous cell carcinoma; SUV_{max}, maximum standardized uptake value; K_1, the forward transport rates of ^{18}F-FDG from plasma to tissue; k_2, the backward transport rates of ^{18}F-FDG from plasma to tissue; v_b, the blood fraction in the tissue; t_d, the voxel-dependent delay time; OR, odds ratio; CI, confidence interval.

(v_b), and AUC (t_d) (Z=2.269, 2.821, 2.848, and 3.276, all P<0.05). When individual parameters were assessed, there was no significant difference in AUC among different parameters (all P>0.05) (*Table 4*, *Figure 4*).

Correlation analysis

SUV_{max} had a moderate positive correlation with the Ki-67 index (r=0.541), while K_1 had a mild positive correlation with the Ki-67 index (r=0.452), and the differences between r (SUV_{max}) and r (k_1) were not significant (Z=0.632, P=0.528). Neither k_2, t_d nor v_b correlated significantly with the Ki-67 index (*Table 5*).

Discussion

SUV is a representative parameter of ^{18}F-FDG PET, and a previous study has shown that TB PET/CT scanners require only a few minutes of scanning to obtain high-quality SUV images, thus enabling effective detection of multiple lesions throughout the body (28). In this study, only data from a total of 3 minutes of scanning between 59 and 61 minutes after ^{18}F-FDG injection were used to generate SUV images, and the results showed that SUV_{max} was significantly higher in malignant lesions and SCC than in benign lesions and AC, respectively, and the diagnostic efficacy reached 0.883 and 0.818, respectively. This was

Table 4 Predictive performance of different parameters

Parameters	AUC (95% CI)	P value	Cutoff	Sensitivity, %	Specificity, %	Comparison with combined diagnosis
Malignant *vs.* benign						
SUV_{max}	0.883 (0.807–0.937)	<0.001	2.200	75.00%	85.00%	Z=1.281, P=0.200
K_1 ($\times 10^{-3}$ mL/g/s)	0.810 (0.723–0.879)	<0.001	1.891	66.67%	83.33%	Z=3.006, P=0.003
k_2 ($\times 10^{-2}$ s^{-1})	0.617 (0.468–0.670)	0.055	–	–	–	–
t_d (s)	0.547 (0.449–0.643)	0.399	–	–	–	–
v_b ($\times 10^{-2}$)	0.746 (0.653–0.825)	<0.001	13.020	58.33%	81.67%	Z=3.965, P<0.001
Combined diagnosis 1	0.909 (0.839–0.956)	<0.001	–	75.00%	90.00%	–
SCC *vs.* AC						
SUV_{max}	0.818 (0.680–0.914)	<0.001	5.520	83.33%	73.33%	Z=2.269, P=0.023
K_1 ($\times 10^{-3}$ mL/g/s)	0.770 (0.626–0.879)	<0.001	2.453	94.44%	46.67%	Z=2.821, P=0.005
k_2 ($\times 10^{-2}$ s^{-1})	0.650 (0.499–0.782)	0.100	–	–	–	–
t_d (s)	0.669 (0.510–0.791)	0.049	–25.700	61.11%	76.67%	Z=3.276, P=0.001
v_b ($\times 10^{-2}$)	0.737 (0.590–0.853)	0.003	5.315	72.22%	76.67%	Z=2.848, P=0.004
Combined diagnosis 2	0.946 (0.840–0.991)	<0.001	–	88.90%	86.70%	–

The combined diagnosis implies the combination of independent predictors, combined diagnosis 1 represents SUV_{max} + K_1 + V_b, and combined diagnosis 2 represents SUV_{max} + K_1 + V_b + t_d. AC, adenocarcinoma; SCC, squamous cell carcinoma; SUV_{max}, maximum standardized uptake value; K_1, the forward transport rates of ^{18}F-FDG from plasma to tissue; k_2, the backward transport rates of ^{18}F-FDG from plasma to tissue; v_b, the blood fraction in the tissue; t_d, the voxel-dependent delay time.

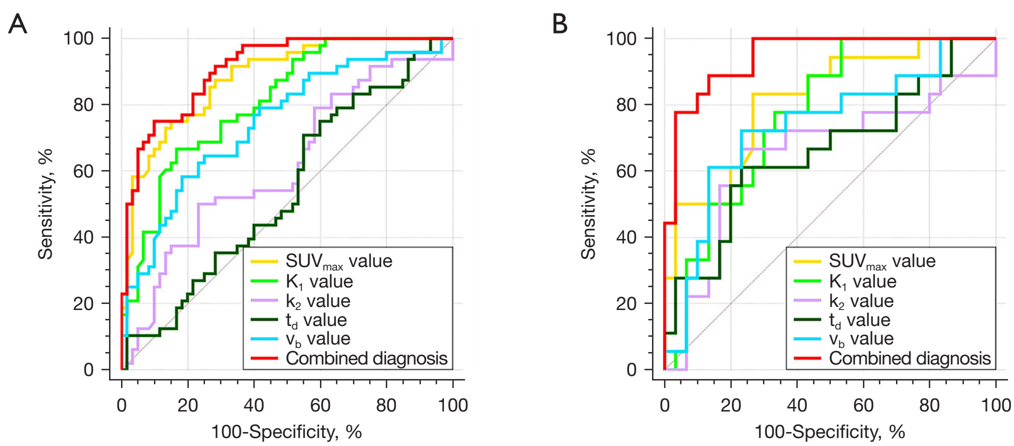

Figure 4 Curves show SUV_{max}, K_1, k_2, t_d, v_b, and the combination of independent predictors by using receiver operating characteristic analysis for (A) differentiation benign and malignant pulmonary lesions and (B) differentiation of adenocarcinoma and squamous cell carcinoma. Details of the area under the curves and 95% CIs of each index are shown in the Results section and *Table 4*. SUV_{max}, maximum standardized uptake value; K_1, the forward transport rates of ^{18}F-FDG from plasma to tissue; k_2, the backward transport rates of ^{18}F-FDG from plasma to tissue; v_b, the blood fraction in the tissue; t_d, the voxel-dependent delay time.

Table 5 Correlation between different parameters and Ki-67 index

Parameters	r value	P value	95% CI
SUV_{max}	0.541	<0.001	0.332–0.698
k_1 ($\times 10^{-3}$ mL/g/s)	0.452	<0.001	0.224–0.634
k_2 ($\times 10^{-2}$ s^{-1})	–0.105	0.426	–0.349–0.153
t_d (s)	0.013	0.919	–0.241–0.267
v_b ($\times 10^{-2}$)	–0.057	0.665	–0.307–0.199

SUV_{max}, maximum standardized uptake value; K_1, the forward transport rates of ^{18}F-FDG from plasma to tissue; k_2, the backward transport rates of ^{18}F-FDG from plasma to tissue; v_b, the blood fraction in the tissue; t_d, the voxel-dependent delay time.

basically consistent with the findings obtained by traditional PET/CT scanning after 20–30 minutes (29,30), indicating that TB PET/CT can effectively differentiate between benign and malignant pulmonary lesions as well as SCC and AC even with a significantly reduced scanning time. The possible reasons are as follows: SUV_{max} was closely related to the proliferation and growth ability of tumor cells. Compared with benign lesions and AC, malignant lesions and SCC have stronger proliferation and growth ability, which leads to increased glucose consumption and uptake and thus a higher SUV_{max} (3,29). In addition, the ultrahigh sensitivity of TB PET/CT may give it the ability to distinguish lesions with small metabolic differences, thus facilitating to some extent the differentiation between benign and malignant lesions and between AC and SCC.

The kinetics parametric imaging used in this study was a nonlinear 1-tissue compartment model proposed by Feng *et al.* (21) that combines the high temporal resolution of TB PET/CT scanners and the clinical need for short-term scans and theoretically requires only a 2-min scan after tracer injection to quantify kinetic indexes. K_1 describes the forward transport rate of ^{18}F-FDG from plasma to tissue, and in general, the more malignant the lesion and the more rapidly the cells proliferate, the greater the K_1 value. In previous works, ^{18}F-FDG K_1, based on the conventional 2-tissue compartment model, has been widely used in the differentiation of benign and malignant lesions (31), the assessment of tumor subgroups (11), and therapy response (32). In the present study, malignant lesions and SCC tended to have more active cell proliferation and metabolic states than benign lesions and AC, so K_1 values increased. This was similar to the results of the abovementioned studies, indicating that the K_1 value obtained from this kinetics parametric imaging of the nonlinear 1-tissue compartment model can provide a reference for the differentiation of benign and malignant lung lesions, as well as SCC and AC in clinical work.

In contrast to K_1, k_2 represents the transport rate of ^{18}F-FDG from tissue to plasma. In a series of studies involving pheochromocytoma (33), soft tissue sarcoma (34), and pancreatic cancer (32), k_2 obtained from the conventional 2-tissue compartment model was proved to be difficult to assess and reflect effectively the lesion information. In our study, although the k_2 values of benign lesions and AC were higher than those for malignant lesions and SCC, respectively, the differences were not statistically significant, which was generally consistent with the abovementioned publications. We hypothesized that this might be due to the low rate of ^{18}F-FDG from tissue to plasma, which makes it difficult for existing methods to detect small differences between different lesions. In addition, Feng *et al.* mentioned in their study that the k_2 value reconstructed by the fast kinetics imaging was less stable, which may also be one of the reasons for the lack of significant differences in k_2 between benign and malignant lung lesions and between SCC and AC in this study (21).

The v_b was associated with the fraction of blood within the lesion. Previous studies have shown that lesions with a high degree of malignancy tend to experience internal blood vessel compression, reduced perfusion, and ultimately decreased v_b values due to reasons such as vigorous proliferation and a tight structure (32,35). In the current study, a significantly decreased v_b was found in both malignant pulmonary lesions and SCC due to the tighter tissue structure, which was in accordance with the mentioned conclusions, indicating that v_b can play a role in the evaluation of lung lesions.

Based on the high temporal resolution and whole-body coverage of TB PET/CT, the nonlinear 1-tissue compartment model-based kinetic parameter imaging introduces the new parameter td, which represents the time required for tracer output from the ascending aorta to different organs of the body. In Feng *et al.*'s study, t_d was longer in the liver, which has a dual blood supply, and in the extremities distant from the ascending aorta, whereas t_d was shorter in the organs with a single blood supply close to the ascending aorta, such as the brain, lungs, and spleen (21). In this study, the t_d values for benign lesions and AC were greater than those for malignant lesions and SCC, respectively, and although the difference was significant only for the latter, it also demonstrated to some extent that t_d has the ability to perform a preliminary assessment of lung lesions. Considering the similarities between benign and malignant lesions and between SCC and AC in terms of the mode of blood supply, the location of the lesion, and the discussion on v_b above, we inferred that the prolonged t_d in the malignant lesion and SCC may be related to poorer perfusion.

The Ki-67 index has important value in reflecting abnormal proliferation and aggressiveness of tumor cells, and some findings suggest that Ki-67 overexpression is closely associated with poor prognosis and rapid disease progression in non-small cell lung cancer (36,37). Previous studies have shown that as Ki-67 expression increases, tumor cell proliferation and metabolism become more active, and the SUV_{max} increases (38), which is consistent with the results of this study, demonstrating that the SUV_{max} based on TB PET/CT can predict the expression of Ki-67 in lung lesions even if the scan time is significantly reduced. In addition, malignant cells may take up more ^{18}F-FDG than normal cells, which may be one of the reasons for the moderate correlation between SUV_{max} and Ki-67. In terms of predicting Ki-67 expression using kinetics ^{18}F-FDG PET/CT-related parameters, both Kajáry *et al.* (11) and Dunnwald *et al.* (39) explored the relationship between transport rate parameters (K_1 and k_2) and the Ki-67 index in breast lesions based on the conventional 2-compartment model, and the results showed no significant correlation between the two parameters and the Ki-67 index. In the current study, K_1 was mildly negatively correlated with the Ki-67 index, and k_2 was not significantly correlated with the Ki-67 index, which is not entirely consistent with the above results. We speculated that this might be related to different tumor types and imaging protocols (40). In addition, this study also showed that neither v_b nor t_d was significantly correlated with Ki-67 expression, suggesting that there were still challenges in the prediction of the Ki-67 index in lung cancer using the nonlinear 1-tissue compartment model-based kinetics parametric imaging.

As one of the most advanced PET imaging methods available, TB PET/CT offers significant advantages over conventional PET/CT. In clinical practice, our experience of using TB-PET/CT has shown that it can significantly reduce scan times, speed up clinical processes, and improve patient comfort. In the assessment of lung cancer, our preliminary study found that the high sensitivity and high resolution of TB PET/CT not only enables the detection of small metastases (41) but also effectively reduces dynamic imaging scan time, facilitating its dissemination in clinical work and thus improving the accuracy of the assessment (42,43). In the future, as TB PET/CT becomes more popular, this combination of comfort and accuracy is expected to provide clinicians with a reliable tool for disease diagnosis and assessment.

Several limitations of our study should be considered. First, this was a single-center study with a relatively small sample size, which might have led to selection bias. Second, there were still few studies on fast kinetics parametric imaging, and the data acquisition and fitting algorithm may still need to be optimized, which reduces the accuracy of the results of this study to a certain extent. Third, due to the lack of relevant software, this study did not generate dynamic parameters based on the conventional two-compartment model, so it is impossible to compare and evaluate dynamic parameters under different models, which may lead to insufficient experimental content.

Conclusions

Quantitative parameters of static imaging and fast kinetics imaging in ^{18}F-FDG total-body PET/CT were able to differentiate benign and malignant pulmonary lesions and SCC and AC, and some of the derived parameters can also predict the Ki-67 index of malignant pulmonary lesions.

Acknowledgments

Funding: This work was supported by the National Key R&D Program of China (No. 2017YFE0103600), the Zhengzhou Collaborative Innovation Major Project (No. 20XTZX05015), the National Natural Science Foundation of China (No. 81720108021), the Zhongyuan Thousand Talents Plan Project - Basic Research Leader Talent (No. ZYQR201810117), the Key Project of Henan Province Medical Science and Technology Project (Nos. LHGJ20220627, LHGJ20190602 and LHGJ20210202), and the Henan Provincial Science and Technology Research Project (No. 212102310689).

Footnote

Reporting Checklist: The authors have completed the STARD reporting checklist. Available at https://qims.amegroups.com/article/view/10.21037/qims-23-186/rc

Conflicts of Interest: All authors have completed the ICMJE uniform disclosure form (available at https://qims.amegroups.com/article/view/10.21037/qims-23-186/coif). TYX and TF report that they are from the commercial company United Imaging Healthcare (UIH), were collaborating scientists providing technical support under the UIH collaboration regulations and had no financial or other conflicts with respect to this study. The other authors have no conflicts of interest to declare.

Ethical Statement: The authors are accountable for all aspects of the work in ensuring that questions related to the accuracy or integrity of any part of the work are appropriately investigated and resolved. The study was conducted in accordance with the Declaration of Helsinki (as revised in 2013). This prospective study complied with ethical committee standards and was approved by the ethics committee of the Henan Provincial People's Hospital & Zhengzhou University People's Hospital (No. 2018067) and informed consent was taken from all individual participants.

References

1. Siegel RL, Miller KD, Fuchs HE, Jemal A. Cancer Statistics, 2021. CA Cancer J Clin 2021;71:7-33. Erratum in: CA Cancer J Clin 2021;71:359.
2. Gould MK, Maclean CC, Kuschner WG, Rydzak CE, Owens DK. Accuracy of positron emission tomography for diagnosis of pulmonary nodules and mass lesions: a meta-analysis. JAMA 2001;285:914-24.
3. Madsen PH, Holdgaard PC, Christensen JB, Høilund-Carlsen PF. Clinical utility of F-18 FDG PET-CT in the initial evaluation of lung cancer. Eur J Nucl Med Mol Imaging 2016;43:2084-97.
4. Luo ZH, Lu PX, Qi WL, Liao FX, Jin AF, Zen QY. Role of (18)F-FDG PET/CT in the diagnosis and management of patients with Langerhans cell histiocytosis. Quant Imaging Med Surg 2022;12:3351-63.
5. Ma G, Zhang X, Wang M, Xu X, Xu B, Guan Z. Role of (18)F-FDG PET/CT in the differential diagnosis of primary benign and malignant unilateral adrenal tumors. Quant Imaging Med Surg 2021;11:2013-8.
6. Fahrni G, Karakatsanis NA, Di Domenicantonio G, Garibotto V, Zaidi H. Does whole-body Patlak (18)F-FDG PET imaging improve lesion detectability in clinical oncology? Eur Radiol 2019;29:4812-21.
7. Boellaard R. Need for standardization of 18F-FDG PET/CT for treatment response assessments. J Nucl Med 2011;52 Suppl 2:93S-100S.
8. Nakajo M, Jinguji M, Aoki M, Tani A, Sato M, Yoshiura T. The clinical value of texture analysis of dual-time-point (18)F-FDG-PET/CT imaging to differentiate be-tween (18)F-FDG-avid benign and malignant pulmonary lesions. Eur Radiol 2020;30:1759-69.
9. Zaidi H, Karakatsanis N. Towards enhanced PET quantification in clinical oncology. Br J Radiol 2018;91:20170508.
10. Tixier F, Vriens D, Cheze-Le Rest C, Hatt M, Disselhorst JA, Oyen WJ, de Geus-Oei LF, Visser EP, Visvikis D. Comparison of Tumor Uptake Heterogeneity Characterization Between Static and Parametric 18F-FDG PET Images in Non-Small Cell Lung Cancer. J Nucl Med 2016;57:1033-9.
11. Kajáry K, Lengyel Z, Tőkés AM, Kulka J, Dank M, Tőkés T. Dynamic FDG-PET/CT in the Initial Staging of Primary Breast Cancer: Clinicopathological Correlations. Pathol Oncol Res 2020;26:997-1006.
12. Yang M, Lin Z, Xu Z, Li D, Lv W, Yang S, Liu Y, Cao Y, Cao Q, Jin H. Influx rate constant of (18)F-FDG increases in metastatic lymph nodes of non-small cell lung cancer patients. Eur J Nucl Med Mol Imaging 2020;47:1198-208.
13. Dimitrakopoulou-Strauss A, Pan L, Sachpekidis C. Kinetic modeling and parametric imaging with dynamic PET for oncological applications: general considerations, current clinical applications, and future perspectives. Eur J Nucl Med Mol Imaging 2021;48:21-39.
14. Rahmim A, Lodge MA, Karakatsanis NA, Panin VY, Zhou Y, McMillan A, Cho S, Zaidi H, Casey ME, Wahl RL. Dynamic whole-body PET imaging: principles, potentials and applications. Eur J Nucl Med Mol Imaging

2019;46:501-18.
15. Badawi RD, Shi H, Hu P, Chen S, Xu T, Price PM, Ding Y, Spencer BA, Nardo L, Liu W, Bao J, Jones T, Li H, Cherry SR. First Human Imaging Studies with the EX-PLORER Total-Body PET Scanner. J Nucl Med 2019;60:299-303.
16. Zhang X, Badawi RD, Cherry SR, Qi J. Theoretical study of the benefit of long axial field-of-view PET on region of interest quantification. Phys Med Biol 2018;63:135010.
17. Cherry SR, Badawi RD, Karp JS, Moses WW, Price P, Jones T. Total-body imaging: Transforming the role of positron emission tomography. Sci Transl Med 2017;9:eaaf6169.
18. Zhang X, Xie Z, Berg E, Judenhofer MS, Liu W, Xu T, et al. Total-Body Dynamic Reconstruction and Parametric Imaging on the uEXPLORER. J Nucl Med 2020;61:285-91.
19. Patlak CS, Blasberg RG. Graphical evaluation of blood-to-brain transfer constants from multiple-time uptake data. Generalizations. J Cereb Blood Flow Metab 1985;5:584-90.
20. Logan J. Graphical analysis of PET data applied to reversible and irreversible tracers. Nucl Med Biol 2000;27:661-70.
21. Feng T, Zhao Y, Shi H, Li H, Zhang X, Wang G, Price PM, Badawi RD, Cherry SR, Jones T. Total-Body Quantitative Parametric Imaging of Early Kinetics of (18) F-FDG. J Nucl Med 2021;62:738-44.
22. Wang D, Zhang X, Liu H, Qiu B, Liu S, Zheng C, Fu J, Mo Y, Chen N, Zhou R, Chu C, Liu F, Guo J, Zhou Y, Zhou Y, Fan W, Liu H. Assessing dynamic metabolic heterogeneity in non-small cell lung cancer patients via ultra-high sensitivity total-body [18F]FDG PET/CT imaging: quantitative analysis of [18F]FDG uptake in primary tumors and metastatic lymph nodes. Eur J Nucl Med Mol Imaging 2022;49:4692-704.
23. Liu G, Xu H, Hu P, Tan H, Zhang Y, Yu H, Li X, Shi H. Kinetic metrics of (18)F-FDG in normal human organs identified by systematic dynamic total-body positron emission tomography. Eur J Nucl Med Mol Imaging 2021;48:2363-72.
24. de Geus-Oei LF, Visser EP, Krabbe PF, van Hoorn BA, Koenders EB, Willemsen AT, Pruim J, Corstens FH, Oyen WJ. Comparison of image-derived and arterial input functions for estimating the rate of glucose metabolism in therapy-monitoring 18F-FDG PET studies. J Nucl Med 2006;47:945-9.
25. Boellaard R, Delgado-Bolton R, Oyen WJ, Giammarile F, Tatsch K, Eschner W, et al. FDG PET/CT: EANM procedure guidelines for tumour imaging: version 2.0. Eur J Nucl Med Mol Imaging 2015;42:328-54.
26. Shieh G. Choosing the best index for the average score intraclass correlation coefficient. Behav Res Methods 2016;48:994-1003.
27. Sun K, Chen X, Chai W, Fei X, Fu C, Yan X, Zhan Y, Chen K, Shen K, Yan F. Breast Cancer: Diffusion Kurtosis MR Imaging-Diagnostic Accuracy and Correlation with Clinical-Pathologic Factors. Radiology 2015;277:46-55.
28. Zhao YM, Li YH, Chen T, Zhang WG, Wang LH, Feng J, Li C, Zhang X, Fan W, Hu YY. Image quality and lesion detectability in low-dose pediatric (18)F-FDG scans using total-body PET/CT. Eur J Nucl Med Mol Imaging 2021;48:3378-85.
29. Deppen SA, Blume JD, Kensinger CD, Morgan AM, Aldrich MC, Massion PP, Walker RC, McPheeters ML, Putnam JB Jr, Grogan EL. Accuracy of FDG-PET to diagnose lung cancer in areas with infectious lung disease: a meta-analysis. JAMA 2014;312:1227-36.
30. de Geus-Oei LF, van Krieken JH, Aliredjo RP, Krabbe PF, Frielink C, Verhagen AF, Boerman OC, Oyen WJ. Biological correlates of FDG uptake in non-small cell lung cancer. Lung Cancer 2007;55:79-87.
31. Dimitrakopoulou-Strauss A, Strauss LG, Heichel T, Wu H, Burger C, Bernd L, Ew-erbeck V. The role of quantitative (18)F-FDG PET studies for the differentiation of malignant and benign bone lesions. J Nucl Med 2002;43:510-8.
32. Epelbaum R, Frenkel A, Haddad R, Sikorski N, Strauss LG, Israel O, Dimitrakopou-lou-Strauss A. Tumor aggressiveness and patient outcome in cancer of the pancreas assessed by dynamic 18F-FDG PET/CT. J Nucl Med 2013;54:12-8.
33. van Berkel A, Vriens D, Visser EP, Janssen MJR, Gotthardt M, Hermus ARMM, Geus-Oei LF, Timmers HJLM. Metabolic Subtyping of Pheochromocytoma and Paraganglioma by (18)F-FDG Pharmacokinetics Using Dynamic PET/CT Scanning. J Nucl Med 2019;60:745-51.
34. Sachpekidis C, Karampinis I, Jakob J, Kasper B, Nowak K, Pilz L, Attenberger U, Gaiser T, Derigs HG, Schwarzbach M, Hohenberger P, Dimitrakopoulou-Strauss A, Ronellenfitsch U. Neoadjuvant Pazopanib Treatment in High-Risk Soft Tissue Sarcoma: A Quantitative Dynamic (18)F-FDG PET/CT Study of the German Interdisc-plinary Sarcoma Group. Cancers (Basel) 2019;11:790.
35. Mankoff DA, Dunnwald LK, Partridge SC, Specht JM. Blood flow-metabolism mismatch: good for the tumor, bad for the patient. Clin Cancer Res 2009;15:5294-6.
36. Wei DM, Chen WJ, Meng RM, Zhao N, Zhang XY, Liao

DY, Chen G. Augmented expression of Ki-67 is correlated with clinicopathological characteristics and prognosis for lung cancer patients: an up-dated systematic review and meta-analysis with 108 studies and 14,732 patients. Respir Res 2018;19:150.
37. Del Gobbo A, Pellegrinelli A, Gaudioso G, Castellani M, Zito Marino F, Franco R, Palleschi A, Nosotti M, Bosari S, Vaira V, Ferrero S. Analysis of NSCLC tumour heterogeneity, proliferative and 18F-FDG PET indices reveals Ki67 prognostic role in adenocarcinomas. Histopathology 2016;68:746-51.
38. Shen G, Ma H, Pang F, Ren P, Kuang A. Correlations of 18F-FDG and 18F-FLT up-take on PET with Ki-67 expression in patients with lung cancer: a meta-analysis. Acta Radiol 2018;59:188-95.
39. Dunnwald LK, Doot RK, Specht JM, Gralow JR, Ellis GK, Livingston RB, Linden HM, Gadi VK, Kurland BF, Schubert EK, Muzi M, Mankoff DA. PET tumor metabolism in locally advanced breast cancer patients undergoing neoadjuvant chemo-therapy: value of static versus kinetic measures of fluorodeoxyglucose uptake. Clin Cancer Res 2011;17:2400-9.
40. Zuo Y, Sarkar S, Corwin MT, Olson K, Badawi RD, Wang G. Structural and practical identifiability of dual-input kinetic modeling in dynamic PET of liver inflammation. Phys Med Biol 2019;64:175023.
41. Fu F, Li X, Wu Y, Xu J, Bai Y, Gao Y, Wang Z, Zhang W, Wei W, El Fakhri G, Shao F, Wang M. Total-body dynamic PET/CT of micro-metastatic lymph node in a patient with lung cancer. Eur J Nucl Med Mol Imaging 2021;48:1678-9.
42. Wu Y, Feng T, Zhao Y, Xu T, Fu F, Huang Z, Meng N, Li H, Shao F, Wang M. Whole-Body Parametric Imaging of (18)F-FDG PET Using uEXPLORER with Reduced Scanning Time. J Nucl Med 2022;63:622-8.
43. Wu Y, Feng T, Shen Y, Fu F, Meng N, Li X, Xu T, Sun T, Gu F, Wu Q, Zhou Y, Han H, Bai Y, Wang M. Total-body parametric imaging using the Patlak model: Feasibility of reduced scan time. Med Phys 2022;49:4529-39.

Cite this article as: Meng N, Zhang M, Ren J, Fu F, Xie B, Wu Y, Li Z, Dai B, Li Y, Feng T, Xu T, Wang M. Quantitative parameters of static imaging and fast kinetics imaging in ^{18}F-FDG totalbody PET/CT for the assessment of histological feature of pulmonary lesions. Quant Imaging Med Surg 2023;13(9):5579-5592. doi: 10.21037/qims-23-186

